MOLECULAR PHYSICS, 1994, VOL. 83, NO. 2, 361–379

Coarse grained spectra, dynamics and quantum phase space structures of H_3^+

By GONZALO GARCÍA DE POLAVIEJA
Departamento de Química, C-IX. Universidad Autónoma de Madrid, Cantoblanco 28049, Madrid, Spain

NICHOLAS G. FULTON and JONATHAN TENNYSON
Department of Physics and Astronomy, University College London, Gower St., London WC1E6BT, UK

(*Received 26 May 1994; accepted 13 June 1994*)

A fully quantum-based assignment system is presented and applied to 3D H_3^+ vibrational calculations. By analysing eigenstates in phase space using the Husimi function, dynamical information is used to find hidden localizations in groups of eigenfunctions. Localization onto several types of periodic orbit is described, including the excited horseshoe motion which has been suggested as an explanation of the features in the H_3^+ photodissociation spectrum of Carrington, A., and Kennedy, R. A., 1984, *J. chem. Phys.*, **81**, 91. However, other localizations are found at the dissociation energy which should not be ignored in the explanation of the Carrington–Kennedy spectrum.

1. Introduction

In this journal in 1982 Carrington, Buttenshaw and Kennedy announced preliminary results for the infrared photodissociation spectrum of H_3^+ [1]. This spectrum contained some 27 000 well resolved transitions in a 220 cm^{-1} region at about 1000 cm^{-1}. Subsequent work [2, 3] has confirmed this spectrum and shown it to vary strongly with isotopic substitution and the kinetic energy of the photodissociated proton. The result which has stimulated most interest is the observation that the coarse-grained photodissociation spectrum shows four peaks each separated by approximately 50 cm^{-1}.

The last decade has seen many theoretical attempts to interpret this spectrum [4–8], based largely on classical or semi-classical dynamics. These studies have shown that, in the H_3^+ dissociation region, classical phase space is dominated by chaotic trajectories. However, one series of periodic trajectories, named the horseshoe, has been discovered [4] and used to explain the coarse-grained regularity in the experimental spectrum [5].

Semiclassical calculations confirmed the existence of the horseshoe states [6], and full three-dimensional (3D) quantal techniques have now been developed which yield energy levels and wavefunctions for the H_3^+ system near dissociation [9, 10]. The horseshoe states have been shown [11] to give high transition probabilities under certain conditions.

Much effort has been denoted to the study of thow eigenfunctions reflect the invariant structures of classical results, and this is the thrust of the persent work. For integrable systems, eigenfunctions are associated with classical invariant tori.

For non-integrable systems, no single association with the classical invariant structures has been devised.

Shnirelman [12] proved that the eigenfunctions of the Laplacian on a compact hyperbolic surface became uniformly distributed in the semiclassical limit except for a set of density zero. Helton and Tabor demonstrated [13] that for general systems eigenfunctions localize onto the regions of phase space associated with classical invariant structures.

A more intuitive approach is due to Voros and Berry [14], who presented the microcanonical hypothesis that describes eigenfunctions as ergodic-like distributions. This hypothesis has been tested by MacDonald and Kaufman in the stadium billiard [15] and has been shown to fail because of the existence of enhanced amplitude along classical unstable periodic orbits [16].

Using Gutzwiller's semiclassical Green's formula expressed as a sum over periodic orbits of the system, Bogomolny [17] and Berry [18] have shown the effect of localization on unstable periodic orbits in ergodic systems in configuration and phase space, respectively.

Many applications to real systems have been performed where eigenstates localize onto classical invariant structures (tori, cantori, unstable and stable periodic orbits, etc.) [19, 20]. Recently, it has been shown that the information concerning classical unstable orbits in classically chaotic systems is contained, in general, in groups of eigenfunctions, and a method to isolate that information has been given [21]. Eigenfunctions previously named as ergodic-like functions can then be shown to contain information about localization.

Two-dimensional time-dependent calculations of initially localized wavepackets have helped our understanding of localization phenomena [22]. Several molecules have been studied in this way, including H_2O [23] and CO_2 [24], but with one of the three vibrational coordinates fixed.

Using information contained in the short term quantum dynamics of H_3^+ we have constructed localized wavefunctions on classical invariant structures. These localized wavefunctions are associated with the bands of coarse-grained spectra. Time-dependent calculations are performed using the full 3D bound eigenstate calculations choosing as the initial centre of the wavepacket maxima of the eigenfunctions in the quantum phase space Husimi representation. An automatic assignment of eigenfunctions is provided for H_3^+ starting from the full 3D discrete variable representation (DVR) calculation. No classical guidance is necessary, although two-dimensional (2D) trajectories are shown to provide complementary verification of the results.

2. Theory

2.1. *Quantum phase space distribution functions*

The solution of a classical conservative N degrees of freedom system is described by the phase trajectory $(q_1(t), \ldots, q_N(t), p_1(t), \ldots, p_N(t))$. Frequently, 2D dynamic problems are studied by means of the Poincaré surface of section (PSOS), the successive interactions of the phase space trajectories with a suitable surface for several initial conditions. General systems show a mixed PSOS of regular Kolmogorov, Arnold and Moser (KAM) tori and chaotic seas.

The difficulty of representing quantum wavefunctions in phase space is due to the uncertainty principle. However, functions resembling phase space distributions have been proved to be useful in quantum mechanical studies.

Wigner [25] introduced the first quantum phase space distribution, known by his name, which for one degree of freedom and for a pure state has the form

$$\rho_W(q, p) = \frac{1}{\pi\hbar}\int_{-\infty}^{\infty} dy \Psi^*(q + y)\Psi(q - y)\exp(2ipy/\hbar). \tag{1}$$

O'Connell and Wigner [26] showed the properties of the distribution. Among others, it has the correct marginal distributions.

$$\int \rho_W \, dp = |\Psi(q)|^2,$$

$$\int \rho_W \, dq = |\Psi(p)|^2, \tag{2}$$

with

$$\int \rho_W \, dp \, dq = 1.$$

However, the result can have negative values. Wigner [27] has shown that any real distribution with the correct marginal distributions will also have negative values for some q and p due to the uncertainty principle. A positive distribution due to Husimi [28] can be obtained by Gaussian smoothing of the Wigner distribution.

$$\rho_H(q, p) = \frac{1}{\pi}\int dp' \, dq' \, \rho_W(q', p') \exp\left(-\left[\frac{(q_i' - q)^2}{2(\Delta q)^2} + \frac{(p_i' - p)^2}{2(\Delta p)^2}\right]\right) \tag{3}$$

$$= \frac{1}{2\pi\hbar}|\langle\psi_{qp}(x)\,|\,\Psi(x)\rangle|^2, \tag{4}$$

with ψ_{qp} the minimum wavepacket taking the form

$$\psi_{qp} = \frac{1}{(2\pi(\Delta q)^2)^{1/4}}\exp\left(\frac{i}{\hbar}px - \frac{(x - q)^2}{4(\Delta q)^2}\right), \tag{5}$$

where

$$\Delta q = \sqrt{\frac{\hbar s}{2}}, \qquad \Delta p = \sqrt{\frac{\hbar}{2}\frac{1}{s}} \qquad s = 1.$$

This distribution can be interpreted as the probability of finding the system in a box centred on (q, p) of size $\hbar/2$. Takahashi [29] and Harriman and Casida [30] have shown that Wigner distributions reveal a quite violent nature, but, on the other hand, the Husimi has a good correspondence with coarse-grained classical calculations.

2.2. *Wavepacket dynamics, power spectra and localization of wavefuntions*

Quantum wavepacket dynamics for a bounded system can be written in terms of the eigenfunctions as

$$\psi(t) = \sum_{n=0}^{\infty} |n\rangle\langle n\,|\,\psi(0)\rangle \exp\left(\frac{-iE_n t}{\hbar}\right) \tag{6}$$

where the initial wavepacket $\psi(0)$ can be taken to be the harmonic oscillator coherent state, and $|n\rangle$ is the nth eigenstate. Applying the Fourier transform to both sides of

(6), we can obtain the mth eigenstate (for $\hbar = 1$):

$$\lim_{T\to\infty} \frac{1}{2T} \int_{-T}^{T} \mathrm{d}t\, |\psi(t)\rangle \exp(iE_m t) = |m\rangle\langle m|\psi(0)\rangle. \tag{7}$$

The dynamics of wavefunctions have recurrences have infinitely many times [31], and recurrences can be studied by means of correlation functions:

$$f(t) = |\langle\psi(0)|\psi(t)\rangle|^2. \tag{8}$$

Due to the relation between the correlation functions and the spectral function $g(E)$

$$g(E) = \frac{1}{2\pi} \int_{-\infty}^{\infty} \langle\psi(0)|\psi(t)\rangle \exp(iEt)\, \mathrm{d}t = \sum_n |\langle\psi(0)|n\rangle|^2 \delta(E - E_n), \tag{9}$$

it is clear that recurrences in the correlation function $f(t)$ will affect the spectrum. A short term recurrence at time T will make the smoothed spectrum,

$$g_T(E) = \frac{1}{2\pi} \int_{-T}^{T} \langle\psi(0)|\psi(t)\rangle \exp(iEt)\, \mathrm{d}t, \tag{10}$$

exhibit a band structure. Sufficiently localized wavepackets, by Ehrenfest's theorem, have to follow classical trajectories for at least some time. Specifically, a wavepacket initially placed on the phase space point (q, p) corresponding to a short classical periodic orbit that is not too unstable has strong short recurrences in $f(t)$ at times related to the period of the orbit. In this particular case, the corresponding smoothed spectrum $g_T(E)$ will have almost equally spaced bands.

A method of isolating the information on localization of the wavefunctions onto closed orbits has been developed [21]. It is based on calculating the wavefunctions corresponding to a band of the spectrum centred at energy E_B and with lifetime τ by using relation (7) without the limit $T \to \infty$:

$$\psi^{\mathrm{BAND}} \equiv \int_{-\tau}^{+\tau} \mathrm{d}t\, |\psi(t)\rangle \exp(iE_B t) = \sum_{n=0}^{\infty} |n\rangle\langle n|\psi(0)\rangle \frac{\sin([E_B - E_n]\tau)}{\pi(E_B - E_n)\tau}. \tag{11}$$

This band wavefunction Ψ^{BAND} is related to the short term recurrence in $f(t)$, so it is expected to be a wavefunction localized onto the chosen periodic orbit. This can be approximated, to reduce the necessary computation, by considering only the states under any band of the smoothed power spectrum, and reducing the lifetime τ. The resultant localized wavefunction is complex, but for visualization purposes we rotate the wavefunction onto the real axis so that we can see the relevant nodal structure.

The more unstable the periodic orbit is, the larger the widths of bands in the spectrum become and the higher the number of important eigenfunctions contributing to the band wavefunction. Localization information could therefore be hidden among many eigenfunctions.

To check the centre (q, p) of the initial wavepacket $\psi(0)$ the following property can be used. For initial coherent states, the spectrum and the Husimi functions are easily related: for one state $|n\rangle$, the value of Husimi on the point (x, p) is the value of the spectrum function $|\langle\psi(0)|n\rangle|^2$ for that state, for wavepacket initially centred at the same point (x, p). We can choose the centre of the wavepacket as high values of the Husimi function that repeat in several states. Alternatively, classical calculations can give the same information of where to place the initial wavepacket by finding stable and unstable periodic orbits of the system.

2.3. *Jacobi Hamiltonian and Husimi functions for triatomics*

In Jacobi coordinates configurations of a triatomic can be represented by two lengths and an angle. The first length r_1 describes the distance between two of the atoms of mass m_2 and m_3. The second length r_2 describes the distance of the third atom, mass m_1, from the centre of mass of the other two. Finally, θ describes the angle between r_1 and r_2. In these coordinates the classical rotationless Hamiltonian can be written as

$$H = \frac{p_{r_1}^2}{2\mu_1} + \frac{p_{r_2}^2}{2\mu_2} + \left(\frac{1}{r_1^2\mu_1} + \frac{1}{r_2^2\mu_2}\right)\frac{p_\theta^2}{2} + V(r_1, r_2, \theta), \tag{12}$$

where the reduced masses are

$$\mu_1^{-1} = (m_2^{-1} + m_3^{-1}), \qquad \mu_2^{-1} = (m_1^{-1} + (m_2 + m_3)^{-1}). \tag{13}$$

The Jacobi Husimi distribution can be written as the modulus squared overlap of the minimum wavepacket $\psi_{r_1', r_2', \theta', p_{r_1}', p_{r_1}', p_\theta'}$ with the eigenfunction Φ_i:

$$\rho_H(r_1', r_2', \theta', p_{r_1}', p_{r_1}', p_\theta') = |\langle \psi_{r_1', r_2', \theta', p_{r_1}', p_{r_1}', p_\theta'} | \Phi_i \rangle|^2. \tag{14}$$

The eigenfunctions used in this paper are obtained from DVR calculations [10]. This method represents the wavefunctions as amplitudes at points, the points being chosen as the Gaussian quadrature points of the basis functions. The minimum wavepacket is computed using the Gaussian quadrature points of the DVR wavefunction, which means that the integration is a simple sum over a grid of DVR points. The size of the grid is $n_{r_1} \times n_{r_2} \times n_\theta$, where n_{r_1} is the number of points in r_1, n_{r_2} the number of points in r_2 and n_θ the number in the angle. This integration is assumed to be accurate for energies of the wavepacket which are close to the eigenenergies of the wavefunctions.

The Husimi value for a point is therefore calculated as

$$\rho_H(r_1', r_2', \theta', p_{r_1}', p_{r_1}', p_\theta') = \left| \sum_{i=1}^{n_{r_1}} \sum_{j=1}^{n_{r_2}} \sum_{k=1}^{n_\theta} \Phi_i(r_1^i, r_2^j, \theta^k) \times \psi_{r_1', r_2', \theta', p_{r_1}', p_{r_1}', p_\theta'}(r_i^i, r_2^j, \theta^k) \right|^2. \tag{15}$$

Since the θ coordinate momentum is coupled to the r_1 and r_2 coordinates, three coordinates, q_1, q_2 and q_3 and their corresponding momenta are defined as follows:

$$\begin{aligned} q_1 &= r_1, \\ q_2 &= r_2 \cos(\theta), \\ q_3 &= r_2 \sin(\theta), \\ p_{q_1} &= p_{r_1}, \\ p_{q_2} &= (p_{r_2}^2 + p_\theta^2)^{1/2} \cos\left[\theta - \tan^{-1}\left(\frac{p_\theta}{p_{r_2}}\right)\right], \\ p_{q_3} &= (p_{r_2}^2 + p_\theta^2)^{1/2} \sin\left[\theta - \tan^{-1}\left(\frac{p_\theta}{p_{r_2}}\right)\right]. \end{aligned} \tag{16}$$

So the minimum wavepacket is now defined as

$$\psi_{r_1', r_2', \theta', p_{r_1'}, p_{r_1'}, p_{\theta'}} = \exp\left(i[q_1 p_{q_1} + q_2 p_{q_2} + q_3 p_{q_3}]\right) \times \exp\left([(q_1 - q_1')^2 + (q_2 - q_2')^2 + (q_3 - q_3')^2]/2\right), \quad (17)$$

where q_1, q_2 and q_3 are the transformed wavefunctions DVR points, and q_1', q_2', q_3', p_{q_1}', p_{q_2}' and p_{q_3}' are the transformed coordinates and momenta defining the position and shape of the minimum wavepacket.

3. Results

In this paper we present results obtained mainly with the H_3^+ potential energy surface of Meyer, Botschwina and Burton (MBB) [33]. We have analysed full 3D eigenvectors calculated using the DVR3D program [32] in Jacobi coordinates. The details of the calculations can be found in [10], which presents the energies and symmetry assignments of all the bound states of H_3^+. We used eigenvectors from extended calculations which has final Hamiltonians of size 8500 and 10000 for the even and odd symmetries, respectively. Although H_3^+ has D_{3h} symmetry the DVR3D program uses C_{2v} symmetry. This splits the calculations into two symmetry blocks by considering odd and even parities in the angular coordinate. Most of the results presented here are with the angle fixed on the C_{2v} symmetry plane, $\theta = 90°$, with no momentum in the angle. This means that only even symmetry eigenvectors need to be studied; the odd symmetries require non-zero θ momentum for non-zero overlap of the wavepacket. For the odd states, equivalent cuts can be performed with no θ momentum by permuting the atoms so the cut no longer lies along the symmetry plane; more discussion of this can be found in section 3.4.

3.1. *Selection of initial points*

As discussed in section 2.2, high values of the Husimi function, equations (14) and (15), can be chosen as centres of wavepacket propagation. The Husimi has $2N - 1$ dimensions, where N is the number of wavefunction dimensions. One dimension is lost since energy must be conserved. We have studied wavepacket propagation with initial points centred at $\theta = 90°$, $p_\theta = 0$, $r_2 = 10^{-5}\, a_0$, p_{r_2} being obtained from energy conservation.

In figure 1 (*a*) we present the result for a frequent pattern seen with a cut through the Husimi function, using the phase space slice described above. It is clear that there is a peak, represented by the darker region, which is centred at $p_{r_1} = -0{\cdot}34$ au, $r_1 = 5{\cdot}07 a_0$. Figure 1 (*b*) shows the eigenfunction plot for a cut at $\theta = 90°$. This eigenstate, the 567th even state with an energy 33 296·3 cm^{-1} above the ground state, corresponds to the well studied horseshoe motion [4, 6, 11]. Figure 2 (*a*) presents the same Husimi cut for a different recurring pattern, again with the eigenfunction plotted in figure 2 (*b*). This is the 661st even parity state with an energy 34 743·2 cm^{-1} above the ground state. There are two clear peaks, the higher one centred at $p_{r_1} = 0{\cdot}34$ au, $r_1 = 3{\cdot}75\, a_0$, the other at $p_{r_1} = 0{\cdot}0$, $r_1 = 2{\cdot}65\, a_0$. Although the eigenfunction does not show such clear localization, there is some structure around $r_2 = 2{\cdot}8\, a_0$.

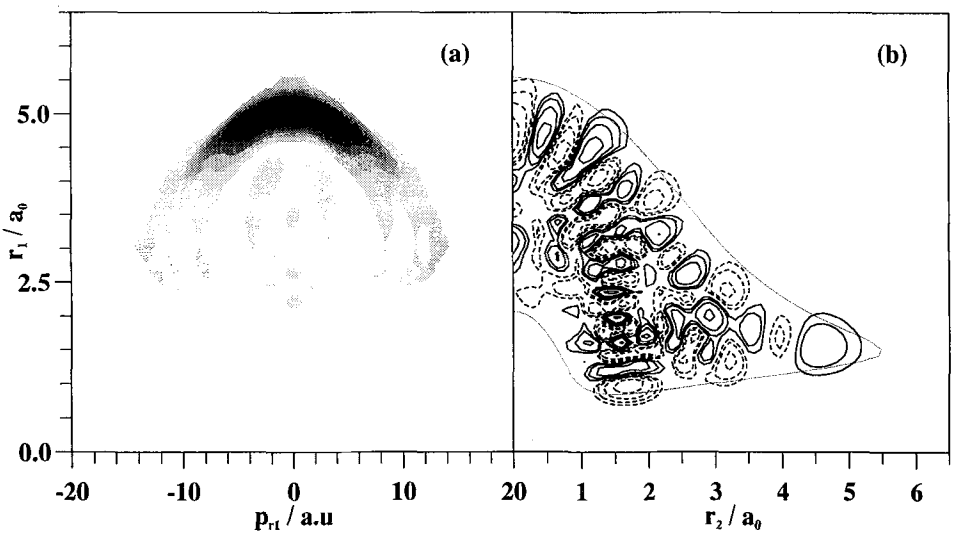

Figure 1. (*a*) r_1 versus p_{r_1} Husimi plot of the 567th even parity H_3^+ wavefunction with an energy 33 296·3 cm^{-1} from the ground state. Fixed coordinates are $\theta = 90°$, $p_\theta = 0$, $r_2 = 10^{-5}\ a_0$ and p_{r_2} obtained from the energy. Darker regions in the plot indicate higher amplitudes. (*b*) r_1 versus r_2 for the same wavefunction and $\theta = 90°$. Positive and negative amplitudes are indicated with the solid and broken contours, respectively, and the faint line indicates the classical turning point for the energy.

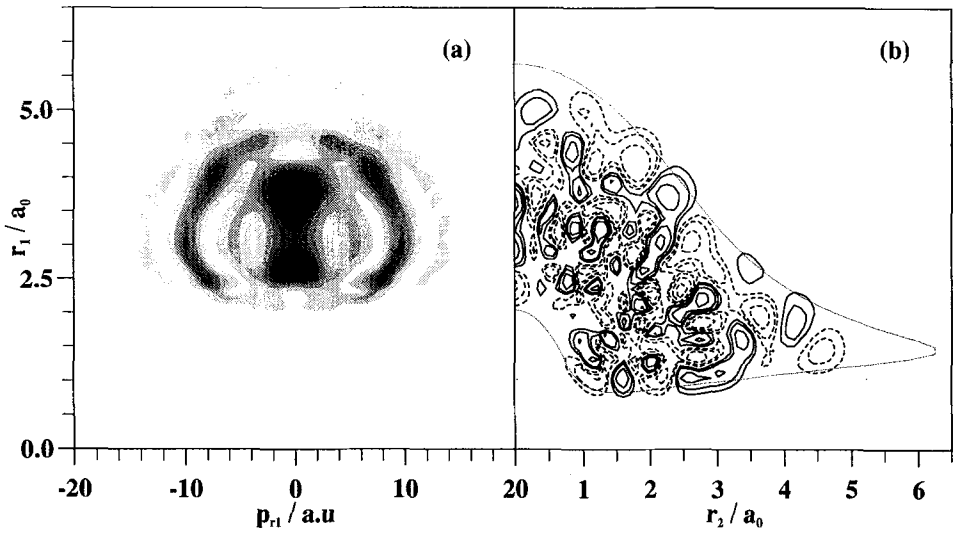

Figure 2. (*a*) r_1 versus p_{r_1} Husimi plot of the 661st even parity H_3^+ wavefunction with an energy 34 743·2 cm^{-1} from the ground state. Fixed coordinates are $\theta = 90°$, $p_\theta = 0$, $r_2 = 10^{-5}\ a_0$ and p_{r_2} obtained from the energy. Darker regions in the plot indicate higher amplitudes. (*b*) r_1 versus r_2 for the wavefunction and $\theta = 90°$. Contours as in figure 1.

3.2. *Correlation functions and power spectra*

Results concerning wavepacket propagation can be studied using the correlation function, equation (8). Figure 3 (*a*,*b*) presents the correlation functions for wave-

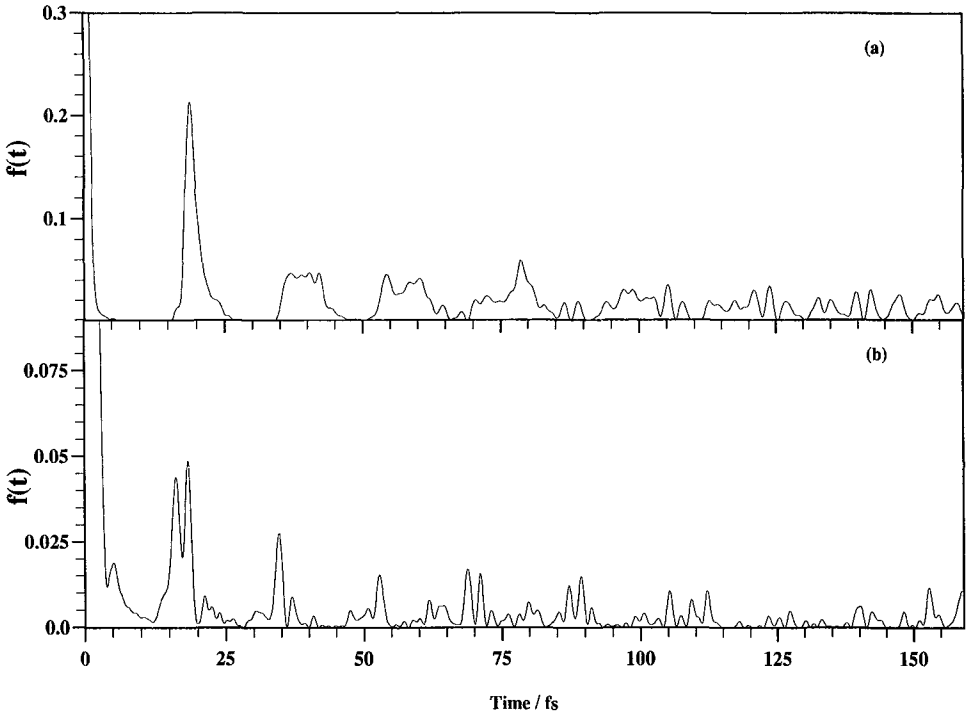

Figure 3. Correlation functions for (*a*) H_3^+ even parity wavepacket with momenta $p_{r_1} = -0{\cdot}34$ au, $p_{r_2} = 7{\cdot}62$ au, $p_\theta = 0$ centred at $r_1 = 5{\cdot}07\ a_0$, $r_2 = 10^{-5}\ a_0$, $\theta = 90°$, and (*b*) H_3^+ even parity wavepacket with momenta $p_{r_1} = 0{\cdot}34$ au, $p_{r_2} = 15{\cdot}40$ au, $p_\theta = 0$ centred at $r_1 = 3{\cdot}75\ a_0$, $r_2 = 10^{-5}\ a_0$, $\theta = 90°$. Note that the vertical scale is different for (*a*) and (*b*); both have an off-scale maximum at 1·0 for the $T = 0$ peak. Recurrences in the wavepacket propagation appear as peaks.

packets centred at points $p_{r_1} = -0{\cdot}34$ au, $r_1 = 5{\cdot}07\ a_0$ and $p_{r_1} = -0{\cdot}34$ au, $r_1 = 3{\cdot}75\ a_0$ found in the previous section. Although they both show decay, in figure 3 (*a*) the recurrence of period $T = 18$ fs for short times gives rise to broad peaks; however, after a lifetime $\tau \approx 70$ fs a more complicated structure arises. In figure 3 (*b*) along with the recurrence of period $T = 18$ fs there is a shorter period recurrence $T = 16{\cdot}5$ fs, and again the decay has a lifetime $\tau \approx 70$ fs. The corresponding power spectra, equation (9), are shown in figure 4 (*a*,*b*). The lower spectrum, figure 4 (*c*), is due to Le Seuer *et al.* [11], and shows the Einstein A coefficient of transition from all the higher even vibrational states to the second excited even-parity state, assigned $(0, 1^1)$, $3178{\cdot}36\ \text{cm}^{-1}$ above the ground state.

The similarity of the position of the peaks in figure 4 (*a*) and (*c*) is convincing, and confirms the idea that the high probability transitions from a low lying state are due to horseshoe states. We have also superimposed, on the power spectra, the smoothed spectrum, equation (10), for time $T = 24$ fs, chosen as a time slightly greater than the first peak in the correlation function, figure 3 (*a*). For figure 4 (*b*) at low energy the peaks coincide with those in figure 4 (*a*), but at higher energies the peaks are separated by a large energy gap, which gives the shorter period recurrence seen in figure 3 (*b*). A smoothed spectrum is added, equation (10), again for a time $T = 24$ fs. As discussed in section 2.2, short recurrences in the correlation function

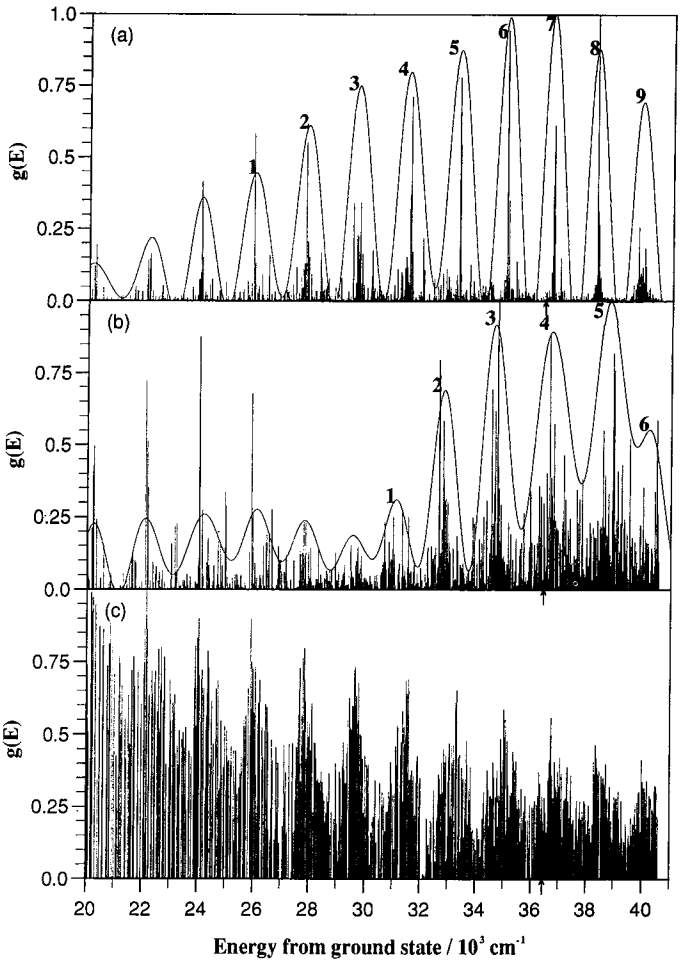

Figure 4. Power spectra for H_3^+ even parity wavepackets with (*a*) momenta $p_{r_1} = -0{\cdot}34$ au, $p_{r_2} = 7{\cdot}63$ au, $p_\theta = 0$ centred at $r_1 = 5{\cdot}07\ a_0$, $r_2 = 10^{-5}\ a_0$, $\theta = 90°$, and (*b*) $p_{r_1} = 0{\cdot}34$ au, $p_{r_2} = 15{\cdot}40$ au, $p_\theta = 0$ centred at $r_1 = 3{\cdot}75\ a_0$, $r_2 = 10^{-5}\ a_0$, $\theta = 90°$. Also plotted is the smoothed spectrum for a time $T = 24$ fs. (*c*) Shows Einstein A coefficients for H_3^+ transitions to the $(0, 1^1)$ state from higher even parity vibrational states [11]. Note the close coincidence of peaks in all three spectra for energies less than 30 000 cm^{-1}. Above 30 000 cm^{-1} the peaks in plot (*b*) differ from the other two. The small arrow marks dissociation; it is clear that the peaks continue above thus energy. The numbers on the peaks in (*a*) and (*b*) mark the peaks which were combined to form localized wavefunctions, figure 5.

give rise to band structure in the power spectra, with peak separation $2\pi k/T$, where conversion from wavenumbers to femtoseconds gives $k = 5308{\cdot}72$ cm^{-1} fs^{-1}. The width of a band is related to the lifetimes in a similar fashion.

3.3. *Localized wavefunctions*

Automatic assignment of the bands in the coarse-grained power spectra can be performed using the band wavefunctions defined in equation (11). Using the

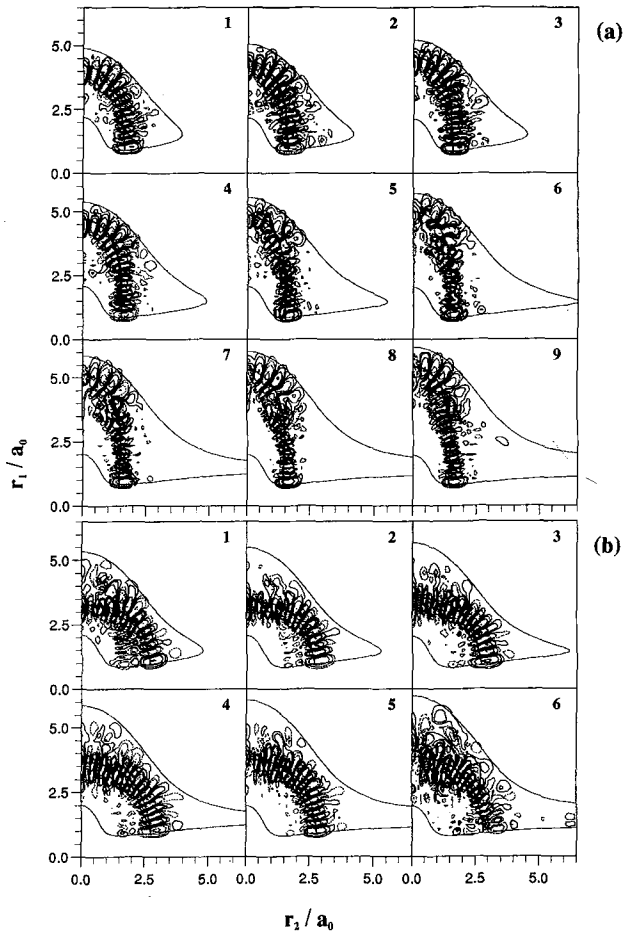

Figure 5. Band wavefunctions corresponding to the numbered peaks in the power spectra are shown in plots (*a*) and (*b*) for figure 4(*a*) and (*b*), respectively. In (*a*) the wavefunctions are horseshoes and a classical horseshoe trajectory is added with an energy corresponding to the centre of the band. The classical turning point at the band centre is also given. This shows the motion is localized and does not fill all the available space. In (*b*) *new* 'elephant foot' wavefunctions are shown and again the corresponding classical trajectory is added. The localization is different from the horseshoe motion, being wider and flatter.

approximation of combining only the states under a single band we have used lifetimes $\tau = 30$ fs and $\tau = 22$ fs for figure 4, parts (*a*) and (*b*), respectively. Figure 5(*a*) presents the band wavefunctions corresponding to nine bands, numbered in energy order, in the horseshoe smoothed power spectrum shown in figure 4(*a*). We have performed classical trajectory analysis of H_3^+ using the MBB potential energy surface, and the classical horseshoe periodic orbit is added to the band wavefunctions, its energy being taken as the centre of the band. Full classical analysis including bifurcation diagrams [34], Poincaré surfaces of section and other periodic orbits will be presented elsewhere [35].

The wavefunction can be seen to localize strongly along the periodic orbit; however, at energies above dissociation, 36 397·1 cm^{-1} above the ground state,

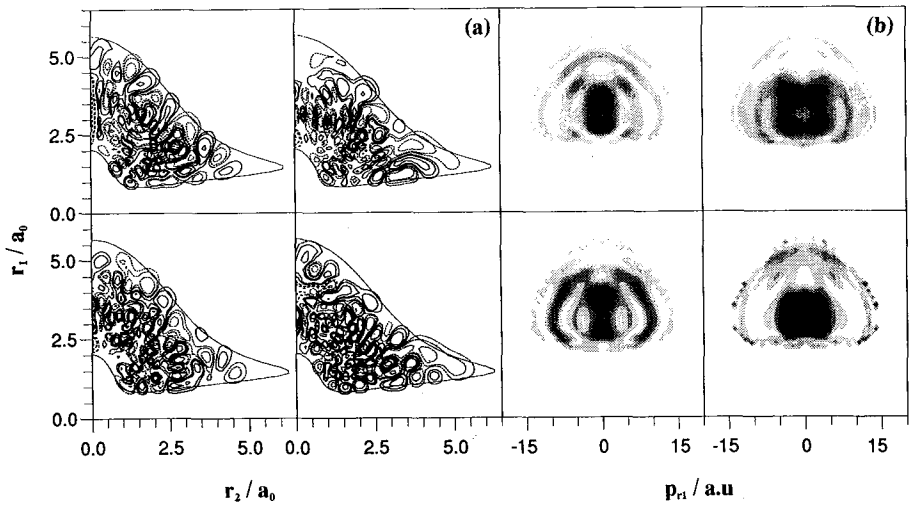

Figure 6. The four states giving the highest contribution to peak 3 in figure 4(*b*). They are even parity states numbers 647, 657, 661 and 663, with energies 34 552·0, 34 673·3, 34 743·2 and 34 770·4 cm^{-1} above the ground state. The wavefunction plots (*a*) do not seem to have many similarities. In plot (*b*) the r_1 versus p_{r_1} Husimi plots are shown for the four states, with fixed coordinates $\theta = 90°$, $p_\theta = 0$, $r_2 = 10^{-5}\, a_0$ and p_{r_2} obtained from the energy. The four Husimi plots do have similar structure with two peaks at $p_{r_1} = 0$, $r_1 \approx 3{\cdot}75\, a_0$ and $r_1 \approx 2{\cdot}5\, a_0$.

marked by an arrow on the power spectra, the quantum behaviour cannot be explained adequately as localization on a single periodic orbit [35]. Also, our quantal results above the dissociation limit should be considered with caution, as the wavefunctions calculated at these energies are bound, since our DVR calculations used a finite grid and therefore do not include true continuum contributions. Furthermore, comparisons with semi-classical density of state calculations [36] suggest that the DVR calculations are significantly less well converged in this region.

Figure 5(*b*) presents band wavefunctions corresponding to six bands of the smoothed power spectrum in figure 4(*b*). Again a classical periodic orbit is added. This *new* periodic orbit, which we have christened the elephant foot as it is fatter than a horseshoe, arises from a bifurcation, at $\approx 28\,300\ cm^{-1}$ above the ground state [35]. The quantum behaviour again localizes strongly on the periodic orbit, and appears to stay localized above dissociation.

In figure 6(*a*) the four eigenstates contributing most to band 3 in figure 4(*b*) are shown. Figure 5(*b*) shows that the band gives rise to a strongly localized wavefunction; however, the eigenstates do not have very clear localization. In the Husimi distribution of these states, figure 6(*b*), for a cut at $\theta = 90°$, $p_\theta = 0$, $r_2 = 10^{-5}\, a_0$ it is clear that they share the same major features with maxima at $p_{r_1} = 0{\cdot}0$, $r_1 = 3{\cdot}4\, a_0$, and $p_{r_1} = 0{\cdot}0$, $r_1 = 2{\cdot}75\, a_0$. The existence of two maxima in all of the plots is due to the fact that the bifurcation gave rise to two, slightly different periodic orbits, which both give maxima on the Husimi plots. We have studied power spectra for a wavepacket centred on one of the maxima which gives a clear power spectrum. The localized wavefunctions for the other maximum can be formed, but the localization is less strong. This decoupling of periodic orbits from the rest of phase space in quantum mechanics has been studied in the time independent picture by means of Feshbach theory [37].

Note that in both Husimi function plots the maximum amplitude did not occur exactly at $p_{r_1} = 0{\cdot}0$ which we would expect from the shape of the localization. The amount of computer time that it takes to compute the Husimi function made sampling very large numbers of points prohibitively expensive, and there was not a sampling point at $p_{r_1} = 0{\cdot}0$. If the region around the peak is investigated in more detail, the maximum does occur at $p_{r_1} = 0{\cdot}0$; however, the difference does not affect the power spectrum or the shape of the localized wavefuctions.

We have found similar localization in the diatomics in molecule (DIM) [38] H_3^+ potential energy surface to those presented here, with qualitative horseshoe and elephant foot features being reproduced. Classical trajectory studies also lead to the same conclusion that details of the potential do not affect the band localization as the dynamics are affected by mainly the general topology of the potential. Classical calculations using a very simple potential formed from three Morse oscillators between the atoms display the same qualitative features; showing that the horseshoe and elephant foot periodic orbits are robust, and insensitive to changes in the potential.

3.4. *Symmetry considerations*

For all the results presented so far we have fixed the Jacobi angle to 90°. By doing so we consider only the motion in one of three equivalent symmetry planes defined by permutations of the atoms. This has the effect of preferentially selecting E states over A_1 states when they have similar types of wavefunction localization. As an equilateral triangle H_3^+ has a degenerate bend mode in the normal mode model, which give rise to an l quantum number to represent the vibrational angular momentum. At energies below linearity, 9912 cm^{-1} above the ground state, l is a reasonably good quantum number, and analysis of H_3^+ and D_3^+ at these energies has been performed has been [39] showing many of the features predicted by topological considerations. However, for the energies examined here the model is not so simple, but symmetry effects are still apparent.

If the power spectrum shown in figure 4 (*a*) is examined closely one can see that the horseshoe behaviour is contained in several states. If the horseshoe Husimi point $p_{r_1} = -0{\cdot}34$ au, $r_1 = 5{\cdot}085\ a_0$ is chosen but we form a triple centred wavepacket with either E or A_1 symmetry, we can obtain power spectra for the symmeterized motion, again using equation (8). These power spectra are shown in figure 7 (*a*) and (*b*), respectively. If these plots are examined one can see that the number of contributing states with a high value has been reduced. If we now concentrate on the peak at $\approx 33\,000\ cm^{-1}$ and form the band wavefunctions, equation (11), for both power spectra, the difference in localization can be studied. Figure 8 (*a*,*b*) shows horseshoe states of different symmetries plotted in Jacobi and symmetry coordinates. The symmetry coordinates, are defined in terms of the changes in the separation of the atoms ΔR_1, ΔR_2 and ΔR_3, where $\Delta R_i = R_i - R_e$, for $i = 1, 2, 3$ and R_e is the equilibrium separation of the atoms, $R_e = 1{\cdot}65\ a_0$. The symmetric stretch coordinate $S_1 = (\Delta R_1 + \Delta R_2 + \Delta R_3)/\sqrt{3}$, the bend coordinate $S_2 = (2\Delta R_1 - \Delta R_2 - \Delta R_3)/\sqrt{6}$, and the asymmetric stretch coordinate $S_3 = (\Delta R_2 - \Delta R_3)/\sqrt{2}$. In the Jacobi plot the A_1 horseshoe does not have such a well defined localization as the E horseshoe, due to interference between the different symmetry equivalent localization. In the symmetry coordinate plot the degeneracy of the bend S_2 and the asymmetric stretch S_3 can be seen more clearly, with the localization having different amplitude and phase in the equivalent configurations. For the E symmetry wavefunction the major

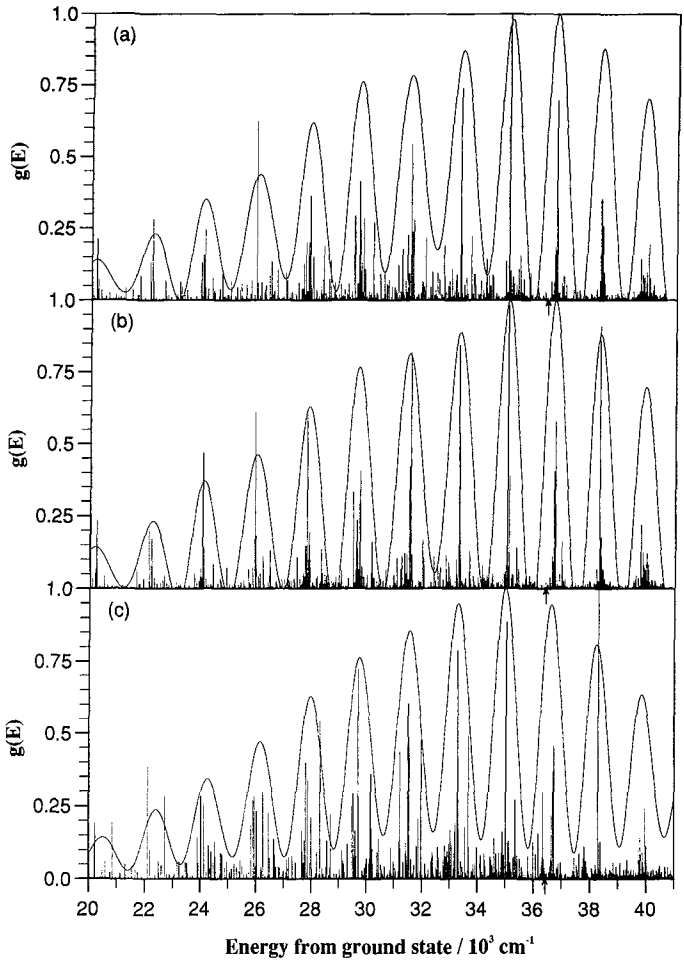

Figure 7. Power spectra for wavepackets with momenta $p_{r_1} = -0{\cdot}34$ au, $p_{r_2} = 7{\cdot}62$ au, $p_\theta = 0$ centred at $r_1 = 5{\cdot}07\ a_0$, $r_2 = 10^{-5}\ a_0$, $\theta = 90°$: (*a*) has even parity E symmetry, (*b*) has A_1 symmetry, and (*c*) has odd parity E symmetry. The smoothed spectrum is also added for a time $T = 24$ fs. The arrow marks the dissociation energy.

amplitude is confined to one region, but in the A_1 wavefunction there is near rotational symmetry, with the same localization in the equivalent configurations.

The symmetry considerations can be taken further if we now look for the odd parity E states. Even state 567 is an E state, and has the same energy as odd state 491. If the Husimi function is studied for this odd parity but with the atoms permuted we obtain, for the same Husimi cut as before, a maximum corresponding to odd symmetry horseshoe motion. If a symmetrized wavepacket is formed for this peak $p_{r_1} = -3{\cdot}72$ au, $r_1 = 4{\cdot}96\ a_0$, a power spectrum can be obtained for the odd parity E horseshoe, shown in figure 7(*c*). If the eigenfunctions under the band at 33 000 cm^{-1} are combined they can be plotted in Jacobi coordinates, except with atoms permuted, and symmetry coordinates. In figure 8(*c*) the interference is clear in the Jacobi plots, and in the symmetry coordinate plot the odd parity is apparent as a reflection though $S_2 = 0$. This time, however, the localization is restricted to two equivalent configurations but with opposite phase.

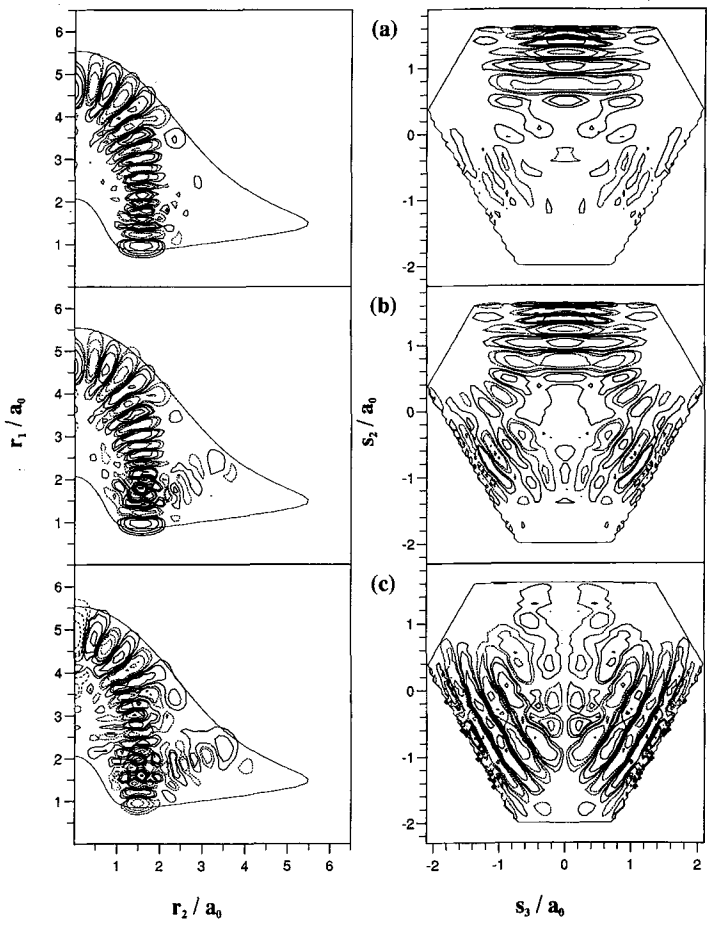

Figure 8. Parts (*a*), (*b*) and (*c*) show band wavefunctions for the peaks centred at $\approx 33\,300\,\mathrm{cm}^{-1}$ in figure 7 (*a*), (*b*) and (*c*), respectively. The plot on the left is in Jacobi coordinates with r_1 versus r_2 and $\theta = 90°$; however, for (*c*) due to a node at $\theta = 90°$ the atoms were permuted. The plot on the right in each case is in symmetry coordinates with S_2 versus S_3 and $S_1 = 0$. Note that in the Jacobi plots the wavefunctions look very similar except for some interference at the equilibrium geometry, $r_1 = 1{\cdot}65\ a_0$, $r_2 = 1{\cdot}43\ a_0$, $\theta = 90°$, whereas in symmetry coordinates the wavefunctions differ considerably.

3.5. *Excited horseshoes*

In their classical analysis of H_3^+, Gomez Llorente and Pollak [5] explain the coarse-grained regularity in the Carrington–Kennedy spectrum [2] as arising from rovibrational transitions from the horseshoe states to similar states with anti-symmetric excitation, i.e., motion out of the $\theta = 90°$ plane. To confirm the existence of these states we have assumed that if the excitation is only one quantum, the strongest localization will be in the odd symmetry calculations with maximum localization near $\theta = 90°$, with a node on the $\theta = 90°$ plane. The power spectrum of such a motion can be obtained by considering a wavepacket moving in the horseshoe motion, just away from the $\theta = 90°$ plane. The initial Husimi point chosen for the wavepacket was $r_1 = 5{\cdot}085\ a_0$, $r_2 = 10^{-5}\ a_0$, $\theta = 78{\cdot}5°$, $p_{r_1} = 0{\cdot}0$, $p_{r_2} = 9{\cdot}1906$ au,

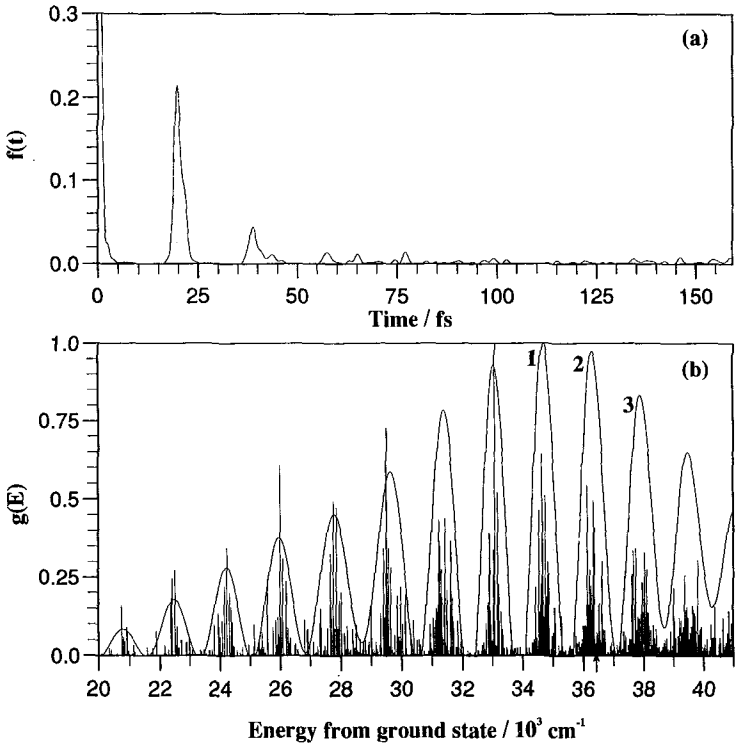

Figure 9. (*a*) Correlation function for an H_3^+ odd parity wavepacket with momenta $p_{r_1} = 0{\cdot}0$, $p_{2_2} = 9{\cdot}1906$ au, $p_\theta = 0{\cdot}0$ centred at $r_1 = 5{\cdot}085\, a_0$, $r_2 = 10^{-5}\, a_0$, $\theta = 78{\cdot}5°$ showing a strong recurrence at 20 fs. (*b*) Power spectrum for the same wavepacket. The smoothed spectrum is for a time $T = 24$ fs. The peaks in this spectrum do not coincide with those in the horseshoe power spectrum in figure 4 (*a*).

$p_\theta = 0{\cdot}0$, and the recurrence function and power spectrum are shown in figure 9 (*a*) and (*b*), respectively. Clearly there is a strong recurrence with a period of 19 fs and a trace of a weaker recurrence of 22 fs.

On the power spectrum a clear structure shows, and interestingly the peaks do not coincide with either the horseshoe, figure 4 (*a*), or the elephant foot, figure 4 (*b*), power spectra. Using equation (11) we can combine the states again under the smoothed power spectrum to reveal localization. In figure 10, 3 states are plotted in Jacobi and symmetry coordinates, corresponding to the peaks labelled in figure 9 (*b*). Due to the node at $\theta = 90°$ the Jacobi 'slice' is with an angle $\theta = 78{\cdot}5°$, however, the same horseshoe shape can be seen. In the symmetry plots it is clear that the node is not simply a symmetry related effect, but splits the localization down the middle. High amplitude is restricted to only one of the 3 symmetry related configurations, but it is likely that both E and A_2 localized wavefunctions can be resolved employing the method described in section 3.4. Preliminary results indicate that there are two excited horseshoe motions with distinctly different band centres, and slightly differing localization, and it is the interference of these two modes that make the Jacobi wavefunction plots appear 'messy'. To compare the relative energies of the motions, table 1 shows the band centres for horseshoe, elephant foot, and the excited horseshoe mode. The energies in cm^{-1} are referred to the vibrational ground state. The bands

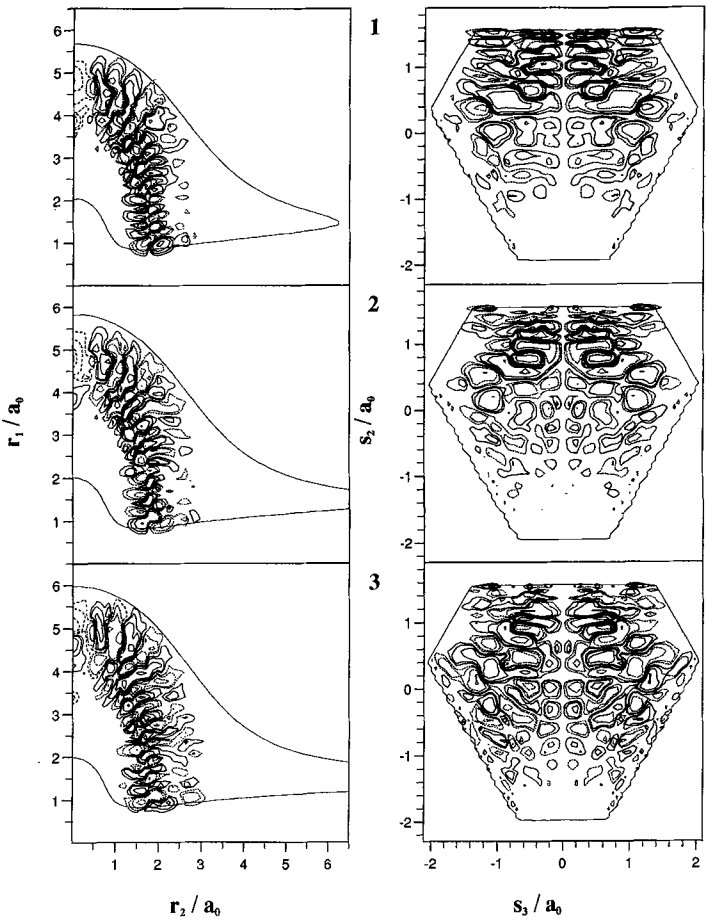

Figure 10. Band wavefunctions under the three numbered peaks in figure 9 (*b*) in Jacobi and symmetry coordinates. The Jacobi plots on the left with r_1 versus r_2 and $\theta = 78{\cdot}5°$ show localization with horseshoe shape; however, the symmetry plots on the right with S_2 versus S_3 and $S_1 =$ show that there is a node along the symmetry plane $\theta = 90°$, and so the wavefunctions are not simple horseshoes.

are ordered in bending node number order, and energy differences are quoted between horseshoe and excited horseshoe, horseshoe and elephant foot, and the horseshoe and the horseshoe with one more node.

4. Conclusion

In this article we have applied Husimi analysis to full 3D calculations on H_3^+ and, by studying repeated phase space features, recovered several types of localization onto classical periodic orbits. The method not only recovers localization which is apparent in eigenvectors, but also motion that does not appear in a single eigenstate. Here we have presented localization on horseshoe, elephant foot and θ excited horseshoe periodic orbits, but have also found strong localization on the symmetric stretch, inverted hyperspherical, symmetric stretch excited horseshoes and

Table 1. Energies of band centres in the smoothed power spectra for the horseshoe E^h, elephant foot E^e and the excited horseshoe E^{exh} motions. All energies are quoted from the ground state. The number of nodes n is obatined from examination of the wavefunctions. As the elephant foot does not exist below 30 000 cm^{-1} the band centres are quoted only in the valid energy window; other peaks in the power spectrum arise from the horseshoe. The difference between the nth horseshoe and excited horseshoe, and the nth horseshoe and elephant foot are also quoted. In the final column the peak separation of the horseshoe is given to show the approximate harmonic progression. Energies marked with a * are above the dissociation energy and should be considered with caution.

n	E_n^h / cm^{-1}	E_n^e / cm^{-1}	E_n^{exh} / cm^{-1}	$E_n^{exh} - E_n^h$ / cm^{-1}	$E_n^e - E_n^h$ / cm^{-1}	$E_{n-1}^h - E_n^h$ / cm^{-1}
11	20 160		22 480	2320		2070
12	22 230		24 220	1990		1840
13	24 070		25 970	1900		1900
14	25 970		27 780	1810		1920
15	27 890		29 650	1760		1800
16	29 690	31 100	31 400	1710	1410	1810
17	31 500	32 840	33 060	1560	1340	1830
18	33 330	34 670	34 690	1360	1340	1730
19	35 060	36 730*	36 310	1250	1670	1650
20	36 710*	38 810*	37 900*	1190	2100	1610
21	38 320*	40 230*	39 490*	1170	1910	1600
22	39 920*		41 345*	1425		

several un-named types of motion, all of which persist up to and above the dissociation energy. The method employed is not classically guided, although classical calculations were performed to demonstrate types of motion. Due to the number of dimensions in phase space one of the momenta has been fixed, partially restricting the allowed motions. As a result of this work, a new method, based on wavepacket recurrence, has now been developed and more complicated orbits have been isolated, including free rotor type motions [40].

The theoretical model currently used to describe the Carrington–Kennedy coarse-grained spectrum of H_3^+ [2] was first proposed by Gomez-Llorente and Pollak [5], based on classical analysis. The main features are explained by transitions from the horseshoe motion, to a similar motion with some excitation out of the $\theta = 90°$ plane. Rotational excitation keeps the dissociation states temporarily bound behind a centrifugal barrier. We have found strong localization on θ excited horseshoe states which preliminary analysis seems to give non-rotational excitation transition frequencies from the corresponding horseshoe state in a range 1200–2000 cm^{-1}. However, we have found many other motions in the dissociating energy range, all with strong power spectra, which cannot be ignored in the explanation of the dissociation mechanism.

The methods we have employed to analyse the motions could be applied to any triatomic species for which eigenvectors can be calculated. The accuracy of the potential is important for quantitative analysis, but for qualitative studies for finding important motions, topologically correct potentials may be adequate.

The authors would like to thank James Henderson for the H_3^+ vectors, Ruth Le

Sueur for the transition spectrum and Tino Borondo for supplying the 'Gear' routine used in the classical trajectory calculations. G.G.P. acknowledges a fellowship from Ministerio de Educacion y Ciencia (Spain) and would like to thank University College London for their hospitality during summer 1993. N.G.F. would like to thank the Science and Engineering Council (SERC) for a studentship. This work has been supported by grants under the British Council—Accione Integrade scheme—and SERC grants for time on the ULCC Convexes and an IBM RS/6000 workstation.

References

[1] Carrington, A., Buttenshaw, J., and Kennedy, R. A., 1982, *Molec. Phys.*, **45**, 753.
[2] Carrington, A., and Kennedy, R. A., 1984, *J. chem. Phys.*, **81**, 91.
[3] Carrington, A., McNab, I. R., and West, Y. D., 1993, *J. chem. Phys.*, **98**, 1073.
[4] Berblinger, M., Pollak, E., and Schlier, Ch., 1988, *J. chem. Phys.*, **88**, 5643.
[5] Gomez-Llorente, J. M., and Pollak, E., 1987, *Chem. Phys. Lett.*, **138**, 125.
[6] Gomez-Llorente, J. M., Zakrzewski, J., Taylor, H. S., and Kulander, K. C., 1988, *J. chem. Phys.*, **89**, 5959,
[7] Child, M. S., 1986, *J. chem. Phys.*, **90**, 3595.
[8] Pfeiffer, R., and Child, M. S., 1987, *Molec. Phys.*, **60**, 1367.
[9] Henderson, J. R., and Tennyson, J., 1990, *Chem. Phys. Lett.*, **173**, 133.
[10] Henderson, J. R., Tennyson, J., and Sutcliffe, B. T., 1993, *J. chem. Phys.*, **98**, 7191.
[11] Le Sueur, C. R., Henderson, J. R., and Tennyson, J., 1993, *Chem. Phys. Lett.*, **206**, 429.
[12] Shnirelman, A. L., 1974, *Ups. Mat. Nauk*, **29**, 1181; see also Zelditch, S., 1987, *Duke Math. J.*, **55**, 919; Colin de Verdiere, Y., 1985, *Commun. Math. Phys.*, **102**, 497.
[13] Helton, J. W., and Tabor, M., 1985, *Physica* D, **14**, 409,
[14] Voros, A., 1977, *Stochastic Behaviour in Classical and Quantum Hamiltonian Systems*, edited by G. Casati and J. Ford (Springer-Verlag); Berry, M. V., 1977, *J. Phys.* A, **10**, 2083.
[15] MacDonald, S. W., and Kaufman, A. N., 1979, *Phys. Rev. Lett.*, **42**, 1189.
[16] MacDonald, S. W., 1983, *Lawrence Berkeley Lab. Rep. LBL*, 14837; Taylor, R. D., and Brumer, P., 1983, *Faraday Discuss. chem. Soc.*, **75**, 170; Heller, E. J., 1984, *Phys. Rev. Lett.*, **53**, 1515.
[17] Bogomolny, E., 1988, *Physica* D, **31**, 169.
[18] Berry, M V., 1989, *Proc. R. Soc. Lond.* A, **423**, 219.
[19] Delande, D., 1991, *Chaos and Quantum Physics*, edited by M.-J. Giannoni, A. Voros, and J. Zinn-Justin, Session LII, 1–31, Les Houches (Elsevier).
[20] Gomez-Llorente, J. M., and Pollak, E., 1992, *Ann. Rev. Phys. Chem.*, **43**, 91.
[21] de Polavieja, G. G., Borondo, F. and Benito, R. M., 1994, *Phys. Rev. Lett.*, in press.
[22] Heller, E. J., 1991, *Chaos and Quantum Phys.*, edited by M.-J. Giannoni, A. Voros, and J. Zinn-Justin, Session LII, 1–31, Les Houches (Elsevier),
[23] Cho, S.-W., and Child, M. S., 1994, *Molec. Phys.*, **81**, 447.
[24] Walton, A. R., and Manolopolous, D. E., unpublished.
[25] Wigner, E., 1932, *Phys. Rev.*, **40**, 749.
[26] O'Connell, R. F., and Wigner, E. P., 1981, *Phys. Lett.* A, **83**, 145.
[27] Wigner, E., 1938, *Trans. Faraday Soc.*, **34**, 29.
[28] Husimi, K., 1940, *Proc. phys. math. Soc. Jap.*, **22**, 264.
[29] Takahashi, K., 1989, *K. Progr. theoret. Phys. Suppl.*, **98**, 109.
[30] Harriman, J. E., and Casida, M. E., 1993, *Int. J. Quantum Chem.*, **45**, 263.
[31] Vilela, Mendes, R., 1991, *J. Phys.* A, **24**, 4349.
[32] Henderson, J. R., Tennyson, J., Le Sueur, C. R. and Miller, S., 1993, *Comp. Phys. Commun.*, **75**, 379.
[33] Meyer, M., Botschwina, P., and Burton, P. G., 1986, *J. chem. Phys.*, **84**, 891.
[34] Farantos, S. C., 1993, *Laser Chem.*, **13**, 87.
[35] Fulton, N. G., Polavieja, G. G. and Tennyson, J., unpublished.
[36] Berblinger, M., Schlier, C., Tennyson, J., and Miller, S., 1992, *J. chem. Phys.*, **96**, 6842.
[37] Taylor, H. S., Zakrzewski, J., and Saini, S., 1988, *Chem. Phys. Lett.*, **145**, 555; Taylor,

H. S., and ZAKRZEWSKI, J., (1988), *Phys. Rev.* A, **38,** 3732; GOMEZ-LLORENTE, J. M., ZAKRZEWSKI, J., TAYLOR, H. S., and KULANDER, K. C., 1989, *J. chem. Phys.*, **90,** 1505.
[38] SCHLIER, CH., and VIX, U., 1985, *Chem. Phys.*, **95,** 401.
[39] SADOVSKII, D. A., FULTON, N. G., HENDERSON, J. R., TENNYSON, J., and ZHILINSKII, B. I., 1993, *J. chem. Phys.*, **99,** 906.
[40] POLAVIEJA, G. G., FULTON, N. G., and TENNYSON, J., unpublished.